An *ab initio* study of xenon retention in α-quartz

2010 J. Phys.: Condens. Matter 22 025501

(http://iopscience.iop.org/0953-8984/22/2/025501)

J. Phys.: Condens. Matter **22** (2010) 025501 (10pp) doi:10.1088/0953-8984/22/2/025501

An *ab initio* study of xenon retention in α-quartz

M I J Probert

Department of Physics, University of York, Heslington, York YO10 5DD, UK

E-mail: mijp1@york.ac.uk

Received 25 September 2009, in final form 9 November 2009
Published 10 December 2009
Online at stacks.iop.org/JPhysCM/22/025501

Abstract

It has recently been suggested that a significant amount of Xe can be absorbed in α-quartz and that this might be a significant process in the recycling of Xe from the atmosphere to the interior of the Earth. This suggestion is tested by *ab initio* calculations of Xe in α-quartz using DFT. Three distinct candidate sites for Xe absorption are identified—substitutional at the silicon vacancy (Xe@V_{Si}), at the oxygen vacancy (Xe@V_O) and at an interstitial site (Xe@I)—and each is shown to be mechanically stable at both $P = 0$ and 2 GPa. The energetics and electronic properties of these defect structures are analysed and it is shown that there is an energy barrier to the absorption at all sites at $T = 0$. If the Xe absorption is a single-stage process in a perfect crystal then the lowest formation energy barrier (at both $P = 0$ and 2 GPa) is for Xe@I at the interstitial site. If absorption is a two-stage process due to vacancies being already present at finite temperatures, then the subsequent barrier to Xe absorption is much lower and Xe@V_{Si} has the lowest formation energy. However, it should be expected that there will be a much higher density of oxygen vacancies available for Xe absorption under realistic Earth core conditions and so in this scenario it is to be expected that all three candidate sites should be occupied.

(Some figures in this article are in colour only in the electronic version)

1. Introduction

It has been known for a long time [1] that the relative abundance of Xe in the Earth's atmosphere is a factor of 20 lower than expected from the abundance of the other noble gases (i.e. Ne, Ar and Kr). An interesting question therefore is 'where has all the missing Xe gone?' In a recent paper, Sanloup *et al* [2] showed in a series of high pressure x-ray diffraction experiments that it was possible for α-quartz to retain a small but significant amount of Xe, and hence suggested that the missing Xe might be absorbed within quartz-like minerals many km below the Earth's surface. It has previously been shown that the missing Xe cannot be trapped in the mantle [3] or in the core [4], and studies on ices [5], clathrates [6] and sediments [7] have also proved negative. Holland *et al* [8] have suggested that Xe might be recycled from seawater via subduction zones into the mantle and then back into the atmosphere via degassing from magma. Hence Sanloup's suggestion is a very interesting one.

Whilst the noble gases are notoriously chemically inert, it is known that Xe is the most reactive one, and has been shown to form a small number of chemical compounds with F, O, C, N, S and the halogens [9]. There are also a small number of examples of Xe being encapsulated in clathrates and zeolites [10]. In particular, it can form the thermodynamically unstable compounds XeO_3 and XeO_4, which therefore led Sanloup *et al* to propose that Xe could occupy Si-vacancy sites within quartz-like materials.

In this paper, this hypothesis is tested by performing a series of *ab initio* total energy calculations of α-quartz with various possible sites for an Xe defect.

2. Method

Total energy calculations were performed using the plane wave pseudopotential density functional theory (DFT) code CASTEP [11, 12]. The basic methodology is well known [13] and has been used many times before for defect calculations (e.g. [14]). In this paper, the PW91 generalized gradient approximation (GGA) [15] with ultrasoft potentials [16] is used, as supplied in the CASTEP library. Where appropriate, structural optimizations of both ionic positions and cell vectors are performed using a modified BFGS-like scheme [17].

All electronic structure calculations are converged to a high degree before any ionic relaxation is attempted using a plane wave cutoff energy of at least 400 eV, a Brillouin zone sampling density of at least $2\pi \times 0.04$ Å^{-1} and an SCF convergence tolerance of at least 10^{-8} eV/atom. Ionic relaxation proceeds until the largest force on any atom is less than 0.01 eV Å^{-1} in magnitude and the corresponding enthalpy change is less than 1×10^{-6} eV/atom. For cell relaxation calculations, the additional constraint is that the largest component of the stress tensor must be less than 0.01 GPa at convergence. All calculations are performed at zero temperature: where this is likely to lead to a difference with experimental results then this will be commented upon.

The Gibbs free energy of the system, in contact with a particle reservoir, is given by

$$G(T, P) = U + PV - TS = H - TS, \tag{1}$$

where U is the internal energy, H is the enthalpy and S the entropy. The chemical potential for a given species of atom j is defined as

$$\mu_j = \frac{\partial G(T, P)}{\partial n_j}, \tag{2}$$

where n_j is the number of atoms of species j. Hence the formation energy of a defect (neglecting entropic contributions) is given by

$$E_{\text{form}} = G_{\text{defect}} - G_{\text{ideal}} = H_{\text{defect}} - H_{\text{ideal}} + \sum_j n_j \mu_j^{\text{removed}} - \sum_j n_j \mu_j^{\text{added}} - n_e \mu_e, \tag{3}$$

where μ^{removed} is the chemical potential of the reservoir where removed atoms are put, μ^{added} is the chemical potential of the reservoir where additional atoms are taken from and μ_e is the chemical potential of electrons for a charged defect. In this work only neutral defects are considered and hence the last term may be neglected

For a compound material such as α-quartz, the chemical potential of the material is determined by the SiO_2 unit:

$$\mu_{SiO_2} = \mu_{Si} + \mu_{O_2} = \mu^*_{Si} + \mu^*_{O_2} + \Delta H_{SiO_2} \tag{4}$$

where μ^*_{Si} is the chemical potential of Si in pure (bulk crystalline) form, $\mu^*_{O_2}$ is the chemical potential of O in pure (diatomic gas) form and ΔH_{SiO_2} is the enthalpy of formation of SiO_2. Hence the chemical potentials of individual Si and O atoms in α-quartz may vary:

$$\begin{aligned} \mu^*_{Si} + \Delta H_{SiO_2} \leqslant \mu_{Si} \leqslant \mu^*_{Si} \\ \tfrac{1}{2}\mu^*_{O_2} + \tfrac{1}{2}\Delta H_{SiO_2} \leqslant \mu_O \leqslant \tfrac{1}{2}\mu^*_{O_2} \end{aligned} \tag{5}$$

and so there will be a range of formation energies, depending on the environment, e.g. Si-rich, O_2-rich, etc. Using the DFT convergence parameters given above, it is found that $\Delta H_{SiO_2} = -10.616$ eV at 0 GPa and $\Delta H_{SiO_2} = -10.382$ eV at 2 GPa.

2.1. Validation

Xe is an unusual element to include in a DFT calculation, and as GGA-DFT does not adequately describe van der Waals interactions, it makes no sense to attempt to validate the Xe pseudopotential and the total energy methodology by calculating the properties of bulk Xe. However, there is some experimental data on the structure of the XeO_4 molecule, and so that will be used for validation instead. Experimentally, it is known that XeO_4 is tetrahedral [18] with an Xe–O bond length of 1.736 Å in the gas phase at ambient conditions.

Total energy calculations and ionic relaxations of the XeO_4 molecule were performed within a cubic supercell, and convergence w.r.t. the size of the supercell was tested with gamma-point-only Brillouin zone sampling, in order to properly describe a gas phase molecule. The Xe ultrasoft pseudopotential explicitly treats all the $5s^25p^6$ electrons. It was found that an 8 Å cubic supercell was sufficient for convergence, yielding a relaxed Xe–O bond length of 1.820 Å (+4.8% w.r.t. experiment). Whilst this is not as accurate as might be hoped for, it gives an indication of the likely accuracy of the subsequent calculations. A Mulliken population analysis [19] showed that the Xe atom has a Mulliken charge of $q^{\text{M}}(\text{Xe}) = +2.92$ and each of the O atoms has $q^{\text{M}}(\text{O}) = -0.73$, and hence the mechanism of the Xe–O bond formation is largely charge transfer. The formation energy of the molecule w.r.t. mono-atomic gas was calculated to be −12.252 eV, which suggests the molecule is reasonably stable, as indeed was found by the stable converged ionic relaxation. If, however, the stability w.r.t. dissociation into O_2 molecules is calculated, then the formation energy becomes +5.328 eV, which suggests that the molecule is only metastable, as known experimentally. We are therefore reasonably confident in our ability to describe Xe–O compounds within DFT-GGA and are not aware of any other DFT calculations of this molecule for comparison.

The validation for α-quartz calculations is much more straightforward, as there is already a substantial literature of such calculations. The only defect in quartz investigated in any depth is that of the O-vacancy [20–23] in various charged states. This seems to be the most obvious defect to be found experimentally as a simple bond-counting picture would suggest a formation energy of the Si vacancy about twice that of the O vacancy, with second-order effects due to electronic and ionic relaxation. There have been no calculations of the Si vacancy until recently, when in a study of amorphous quartz Richard *et al* [23] suggested a substantial energy lowering due to ionic relaxation around the Si vacancy, and so this defect might not be as uncommon as previously expected.

Total energy calculations, with full ionic and cell relaxation, were performed for α-quartz. The experimentally known structure has 6 O and 3 Si atoms per conventional hexagonal unit cell with $P3_221$ symmetry. The relaxed theoretical minimum enthalpy structures are given in table 1. The zero pressure DFT-LDA has lattice parameters −1.4% w.r.t. experiment and DFT-GGA +1.6% w.r.t. experiment which is a commonly observed trend.

Table 1. Relaxed cell parameters for α-quartz.

	a, b (Å)	c (Å)	c/a	volume (Å^3)
LDA, $P = 0$	4.842	5.331	1.1011	108.2
GGA, $P = 0$	4.990	5.465	1.0951	117.9
expt, $P = 0$	4.910	5.402	1.1002	112.8
LDA, $P = 2$ GPa	4.753	5.260	1.1068	102.9
GGA, $P = 2$ GPa	4.871	5.349	1.0983	109.9

2.2. *Preliminary study*

The above formalism was used to calculate the vacancy formation energies in a conventional nine-atom α-quartz cell. This corresponds to an unrealistically high density of vacancies, and a proper calculation of an isolated vacancy would have to perform a rigorous finite-size supercell scaling study. The following standard notation is used: V_{Si} for a vacancy at the silicon site, etc. In all cases it is important to allow for cell relaxation in the presence of the defect: for the finite pressure case this relaxation will do work against the external pressure. Obviously, within a small unit cell there will be a considerable finite-size effect, and so the atomic relaxation is not expected to be representative of an isolated defect. The results are given in table 2. Note that the V_O formation energy in this work in an O_2 environment is 6.71 eV, which is comparable to the other published results, but this energy is considerably reduced if the external environment is an SiO_2 reservoir, as can be seen from equation (4). Whilst an O_2 environment might be appropriate for a laboratory-based experiment, an SiO_2 reservoir is more reasonable for an Earth core environment.

Sanloup *et al* [10] hypothesized that the missing Xe is incorporated into quartz at V_{Si} sites. To test this suggestion, a range of possible sites for Xe within this small cell were considered to see which sites might be possible candidates. As well as the V_{Si} and V_O sites, a variety of possible interstitial sites were considered, two of which (labelled here as Xe@I_T and Xe@I_M) are shown in figure 1. The Xe@I_T defect (pre-relaxation) is an interstitial site with six nearest-neighbour Si atoms and two O atoms and is therefore eightfold-coordinated, whilst the Xe@I_M defect is situated at the mid-point between two O atoms and also has four Si neighbours. It was found that, although the unrelaxed interstitial defects were quite distinct, they converged onto the same relaxed structure. The resulting defect formation energies are shown in table 3.

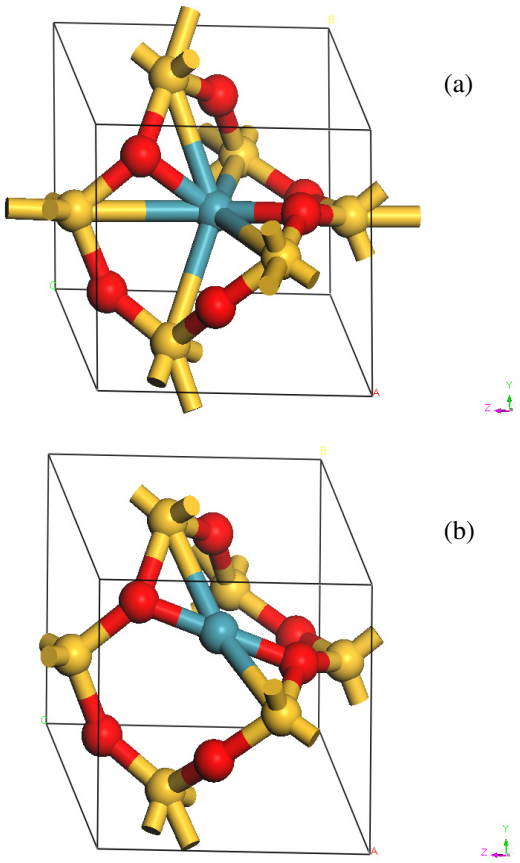

Figure 1. Location of interstitial sites pre-relaxation. (a) shows I_T which is at the centre of the six nearest Si atoms and is eightfold-coordinated, and (b) shows I_M which is at the mid-point between oxygen atoms and also has four Si nearest neighbours.

There is a considerable lattice relaxation in these small cells which might not be representative of an isolated Xe defect. However, whilst there is a wide range of Xe defect formation energies depending on site, it appears that none of the Xe defect sites considered are energetically stable. Note that, whilst the variable external environment can significantly reduce the substitutional defect formation energies, it has no effect on the interstitial sites (as there is only the one Xe gas environment to consider). It is interesting to note that Xe@V_{Si} has the largest volume change (positive expansion of the cell) whilst the interstitial sites have the smallest volume change. Also, whilst the effect of pressure has a small effect on the

Table 2. Vacancy formation energies.

Defect	E_{form} (eV)					
V_{Si}	$5.05 \cdots 15.67$[a]	7.28[b]	4.78[c]			
V_O	$1.40 \cdots 6.71$[a]	6.71[b]	5.71[c]	6.97[d]	$3.58 \cdots 4.58$[e]	$3.58 \cdots 6.63$[f]

[a] This work with nine-atom α-quartz supercell with full range of possible environments.
[b] This work with nine-atom α-quartz supercell with O_2 environment.
[c] Averaged 108-atom amorphous quartz result from [23] with O_2 environment.
[d] 36-atom α-quartz supercell result from [20] with O_2 environment.
[e] $15 \cdots 51$ atom cluster result from [22] as vary embedding method.
[f] 15-atom cluster result from [22] as vary basis set.

Table 3. Xe defect formation energies in nine-atom α-quartz cell.

Defect	E_{form} (eV) Unrelaxed	E_{form} (eV) Relaxed	Final volume (Å^3) (%w.r.t. GGA bulk)
Xe@V_{Si} 0 GPa	29.63 ··· 40.25	3.93 ··· 14.55	169.60 (+43%)
Xe@V_O 0 GP	40.67 ··· 45.98	2.31 ··· 7.62	135.48 (+14.9%)
Xe@I_T 0 GPa	21.68	6.27	127.11 (+7.8%)
Xe@I_M 0 GPa	22.38	6.27	127.47 (+8.2%)
Xe@V_{Si} 2 GP	30.14 ··· 40.52	4.16.. 14.54	132.36 (+20.4%)
Xe@V_O 2 GP	42.50 ··· 47.69	2.66 ··· 7.86	132.26 (+20.3%)
Xe@I_T 2 GPa	22.84	6.41	124.57 (+13.3%)
Xe@I_M 2 GPa	30.18	6.39	124.95 (+13.6%)

formation energy, it has a proportionally larger effect on the volume change. This initial survey also suggested that Xe at the interstitial sites was comparable in formation energy to the vacancy sites and should be considered in more detail. Whilst this defect concentration might seem to be artificially high, it is actually comparable to the initial Xe loading in Sanloup *et al* of 30–40 atomic weight % (wt%) at 1500 K, which they indeed found to be unstable.

3. Results

3.1. Energetics

Whilst the preliminary study used the same Xe defect density as the initial loading of Sanloup *et al*, they reported that an initial Xe loading of 30–40 wt% relaxed to a final concentration of 2.2 wt% at room temperature and pressure. Taking the mass of a conventional three (SiO_2) unit cell as 180 amu and the mass of Xe as 132 amu, this final loading corresponds to an interstitial defect concentration of one Xe atom in 33.3 unit cells. Therefore the defect formation energy in a larger $3 \times 3 \times 3$ supercell was investigated, corresponding to an actual interstitial defect density of 2.7 wt%. Considering Xe at a vacancy rather than an interstitial site changes the defect density by less than 0.02 wt% for this large size supercell. The symmetric $3 \times 3 \times 3$ supercell was chosen to minimize finite-size shape effects. The corresponding defect formation energies will therefore be at approximately the correct density for the experimental situation, and there is no need for a finite-size scaling to establish the dilute limit. Note that, in some substitutional sites, the defect formation energy is higher than the results of table 3 for the smaller cell—this is presumably due to the gross lattice distortions coupling together in the smaller cells, whereas this much larger cell is closer to the dilute limit. As found for the smaller cell, the Xe@I_M defect once again relaxed to the same structure as Xe@I_T, which confirms our basic hypothesis that there is only one unique relaxed interstitial site, Xe@I. All the calculated Xe defect formation energies for this larger supercell are given in table 4.

The first result of interest is that for the vacancy formation energies. Whilst previous works had only considered the exchange of O atoms with an O_2-rich environment (appropriate for α-quartz at the surface of the Earth), in this work the full range of chemical potentials is considered. This shows that there is a considerable reduction in the V_O formation energy for an SiO_2-rich environment, such as would be found within the interior of the Earth. This would greatly increase the density of V_O available.

Table 4. Xe defect formation energy in $3 \times 3 \times 3$ α-quartz supercell. Volume changes are relative to the calculated volume of the $3 \times 3 \times 3$ supercell without Xe using the same computational parameters and pressure.

Defect	E_{form} (eV) (fully relaxed)	Final volume (%w.r.t. GGA bulk)	Final volume (%w.r.t. GGA vacancy)
V_{Si} 0 GPa	4.18 ··· 14.80 4.18[a]	−1.34%	
V_O 0 GPa	1.24 ··· 6.55 6.55[a]	−0.54%	
Xe@V_{Si} 0 GPa	6.01 ··· 16.63 1.83[b]	−0.18%	+1.18%
Xe@V_O 0GPa	6.48 ··· 11.79 5.24[b]	+0.19%	+0.73%
Xe@I_T 0 GPa	5.24	−0.74%	
Xe@I_M 0 GPa	5.24	−0.64%	
V_{Si} 2 GPa	4.49 ··· 14.87 4.49[a]	+0.36%	
V_O 2 GPa	1.07 ··· 6.26 6.26[a]	−0.20%	
Xe@V_{Si} 2 GPa	6.55 ··· 16.93 2.06[b]	+0.42%	+0.06%
Xe@V_O 2 GP	6.94 ··· 12.13 5.87[b]	+1.87%	+2.08%
Xe@I_T 2 GPa	5.29	+1.70%	
Xe@I_M 2 GPa	5.29	+1.53%	

[a] Formation energy w.r.t. O_2 reservoir.

[b] Formation energy w.r.t. pre-formed vacancy.

It should be noted that the experiments of Sanloup *et al* [10] were performed on α-quartz at a range of different temperatures and pressures, from 300 to 2300 K and from 0.5 to 6 GPa. The standard *ab initio* formation energy method used above is for zero temperature. It is well known that α-quartz undergoes a phase transition to coesite above 2 GPa and so the studies in this paper were restricted to Xe in α-quartz at both $P = 0$ and 2 GPa. It would be interesting to extend these studies to finite temperature and to consider a range of other SiO_2 polymorphs, such as amorphous quartz, coesite and stishovite, as all are expected to be found within the mantle region. It has also been recently shown that, even at zero temperature, there is a high pressure amorphization of α-quartz [24]. The study of Richard *et al* [23] showed that there was an effect of different local atomic structures, and that the averaged V_{Si} formation energy in a 108-atom amorphous structure (for an O_2-rich environment) was 4.78 eV. In this work, the corresponding V_{Si} formation energy in a 242-atom α-quartz structure is 4.18 eV. This small difference could be due to the effects of crystalline versus amorphous structure, and/or to the effect of supercell size. Nevertheless, this level of agreement is encouraging and suggests that the results obtained here for α-quartz will also be relevant to other SiO_2 polymorphs and amorphous structures at comparable densities.

It is also interesting to note the effect of pressure on the vacancy formation energies. In the case of an SiO_2-rich

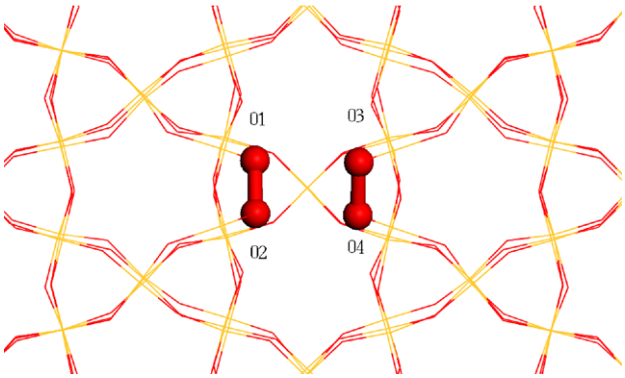

Figure 2. Local structure of the relaxed V_{Si} defect from the $3 \times 3 \times 3$ supercell at 0 GPa.

environment, it is apparent that increasing the pressure from $P = 0$ to 2 GPa has a small effect in increasing the formation energy of V_{Si} and a bigger effect on reducing the formation energy of V_O. However, it is likely that going to even higher pressures will have a diminishing effect on the V_O formation as the volume change does work against the external pressure. Hence it is unclear what will happen in high pressure phases, such as stishovite.

The Xe defect results show that, at both $P = 0$ and 2 GPa, there are no sites for which Xe is stable at $T = 0$ as the defect formation energy is at least 5.2 eV. However, it is possible that the defect at either of the vacancy sites could be formed as a two-stage process. If there were pre-existing vacancies (either V_{Si} or V_O) then the additional energy required to form a Xe defect is considerably reduced. This is shown in the rightmost columns of table 4. In this scenario, the lowest additional energy barrier (V_{Si} site) is now only 1.83 eV. This is therefore still unstable at T=0 but could be easily stabilized under the experimental temperatures of Sanloup *et al* (500 K and above) and in the Earth's interior. There is no two-step process available for the interstitial sites (hereafter collectively referred to as Xe@I).

There is also a small effect of pressure, with higher pressures causing a slight increase in the formation barrier—this is probably due to the large volume change in the non-defective cell going from $P = 0$ to 2 GPa, which means that the high pressure structure has considerably less free volume to accommodate the Xe defect, and hence there is a larger formation energy barrier.

Considering the total energy barriers, it would seem that the interstitial defects Xe@I are most likely, but if there are pre-existing vacancies, the Xe@V_{Si} defect has the lowest additional barrier. However, the energetics of vacancy formation are such that, at finite temperatures, there is likely to be a much higher density of V_O sites. Sanloup *et al* also report an approximate 2% volume expansion at $P = 2$ GPa upon Xe absorption. This is consistent with the calculated volume expansion for Xe@V_O and to a lesser extent with Xe@I, but for Xe@V_{Si} the calculated expansion is much smaller. Hence it is likely that, in the non-ideal crystals and amorphous phases found at high temperature and pressure in the Earth's interior, all three sites will be occupied with varying probability.

Table 5. Local structure of V_{Si}.

P (GPa)	O1–O2 (Å)	O3–O4 (Å)	O1–O3 (Å)	O2–O4 (Å)	O1–O2–O4–O3 (deg)
0	1.481	1.479	2.816	2.781	38.2°
2	1.473	1.474	2.889	2.534	43.8

Table 6. Local electronic structure of V_{Si}.

P (GPa)	q^M (O1)	q^M (O2)	q^M (O3)	q^M (O4)	LUMO (eV)
0	−0.62	−0.61	−0.62	−0.61	3.723
2	−0.62	−0.60	−0.62	−0.60	3.876

3.2. Defect structures

3.2.1. Silicon vacancy. The local structure of the relaxed V_{Si} in the absence of Xe is described by the four neighbouring O atoms as shown in figure 2. The detailed structure is given in table 5. Note that the relaxed O_2 dimer bond length in an 8 Å cubic cell using the same DFT parameters is 1.230 Å (which is +1.6% w.r.t. experiment)—hence it can be seen that the O1–O2 and O3–O4 bonds are slightly longer and therefore weaker, as expected due to the residual bonding with their neighbouring Si atoms. A Mulliken population analysis [19] of the charge density is also performed. Whilst non-defective α-quartz has a Mulliken charge on every O atom of $q^M(O) = -1.2$ and $q^M(Si) = +2.4$ on every Si atom and a DFT-GGA bandgap of 6.8 eV, this is not the case for atoms in the vicinity of a defect. The local electronic structure is detailed in table 6 at both $P = 0$ and 2 GPa. This shows that there is a charge deficiency of 0.59e on each of the four O atoms around the vacancy, which almost exactly cancels the missing Mulliken charge on the missing Si atom and so there is no long-range charge redistribution. That the electronic structure of this defect is localized can be seen in the 3D isosurface plot of the HOMO and LUMO at $P = 0$ GPa, as shown in figure 3.

The DFT-GGA electronic density of states (DOS) for a pure α-quartz system and also for each of the five defects considered is shown in figure 4. The comparison of DOS for pure and V_{Si} shows that the vacancy results in a number of extra (localized) defect states inserted into the bandgap at approximately $E_F + 3.7$ eV and $E_F + 5.3$ eV and a small shoulder in the DOS at E_F. The states at $E_F + 6.0$ eV correspond to a small shift of the equivalent states in the pure system and hence are band-like (delocalized) states.

3.2.2. Oxygen vacancy. The local structure of the relaxed V_O in the absence of Xe is described by the two neighbouring Si atoms as shown in figure 5. The detailed structure is given in table 7 along with the results of the Mulliken charge analysis. In a non-defective α-quartz crystal the Si–Si distance is 3.084 Å—hence there is a considerable local relaxation around this defect. This correlates with the previous observations of a long-ranged lattice deformation out to at least 12 Å from the V_O site [22] and the corresponding difficulty in converging the properties of an isolated V_O with supercell size. In this study, the minimum V_O separation is 14.9 Å and so the deformation

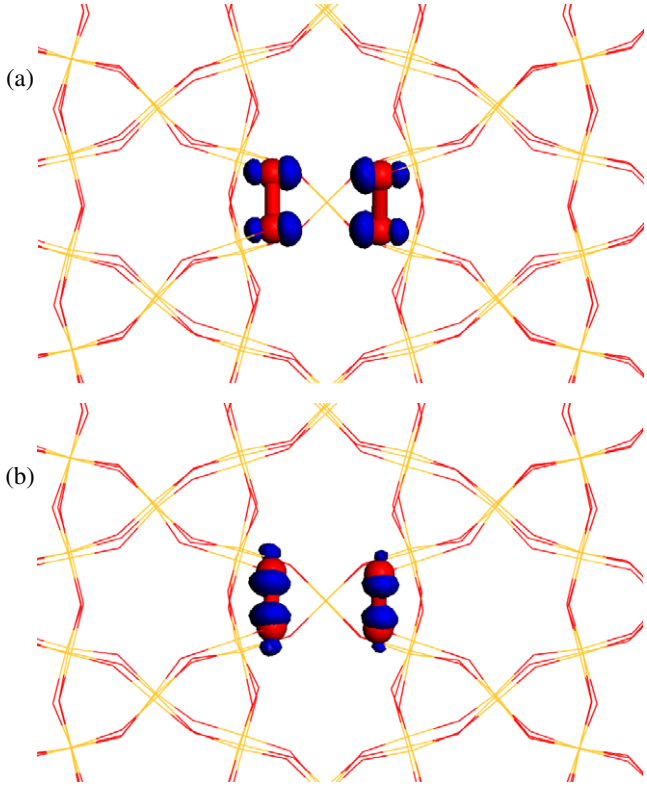

Figure 3. 3D isosurface plot at $\rho = 0.02$ of (a) HOMO and (b) LUMO for V_{Si} from the $3 \times 3 \times 3$ supercell at 0 GPa.

pattern will only be probed out to 7.45 Å due to periodic boundary conditions. However, the aim of this work is to study defects at the experimental concentration of Sanloup *et al*, not to study isolated defects, and so the results presented here are still relevant.

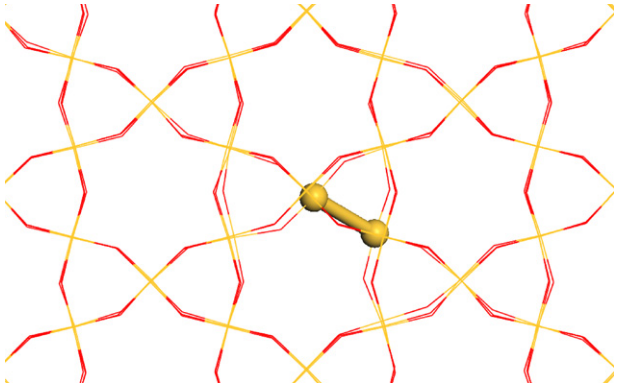

Figure 5. Local structure of the relaxed V_O defect from the $3 \times 3 \times 3$ supercell at 0 GPa.

Table 7. Local structure of V_O.

P (GPa)	Si1–Si2 (Å)	q^M (Si1)	q^M (Si2)	LUMO (eV)
0	2.431	+1.76	+1.76	5.804
2	2.376	+1.77	+1.75	5.923

The 3D isosurface plot of the HOMO and LUMO at $P = 0$ GPa as shown in figure 6 shows that, whilst the HOMO is localized, the LUMO is now delocalized and has a much reduced volume (hence the need to reduce the isosurface value in this figure). This can be understood from the DOS plots of figure 4 where there is no clear picture of extra states in the gap and the LUMO corresponds to the conduction band minima of the pure system.

3.2.3. Xenon at silicon vacancy. If the α-quartz has pre-existing defects such as V_{Si}, then there is only a small additional energy barrier to absorbing a Xe atom, as detailed

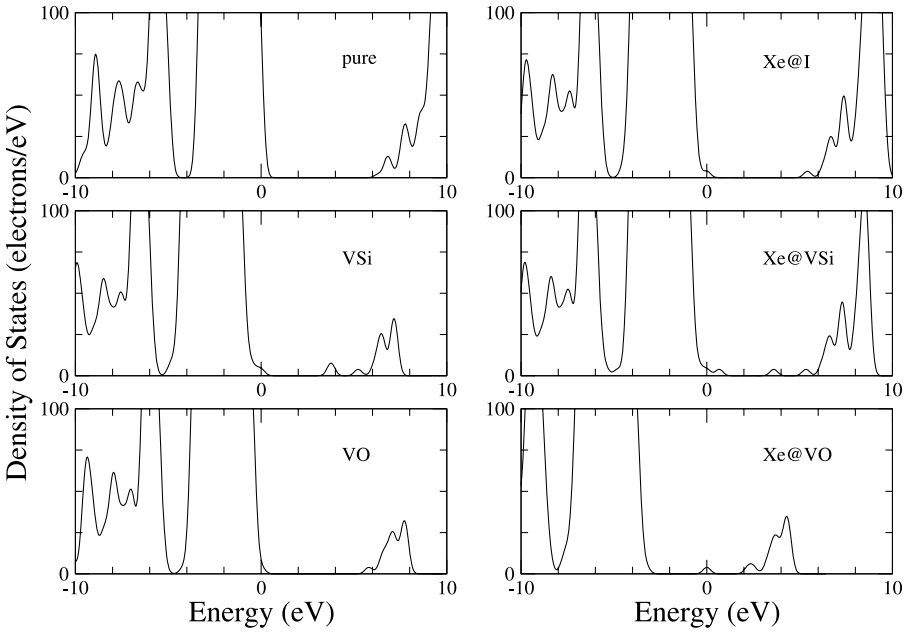

Figure 4. Electronic DOS for pure α-quartz and the various defect states considered.

Table 8. Local structure of $Xe@V_{Si}$.

P (GPa)	Xe–O1 (Å)	Xe–O2 (Å)	Xe–O3 (Å)	Xe–O4 (Å)	O1–Xe–O2 (deg)	O2–Xe–O3 (deg)	O4–Xe–O1–O2 (deg)	O4–Xe–O3–O2 (deg)
0	2.338	2.002	2.281	1.997	89.5	90.6	179.2	179.2
2	2.295	1.994	2.251	1.996	86.6	89.2	176.4	177.2

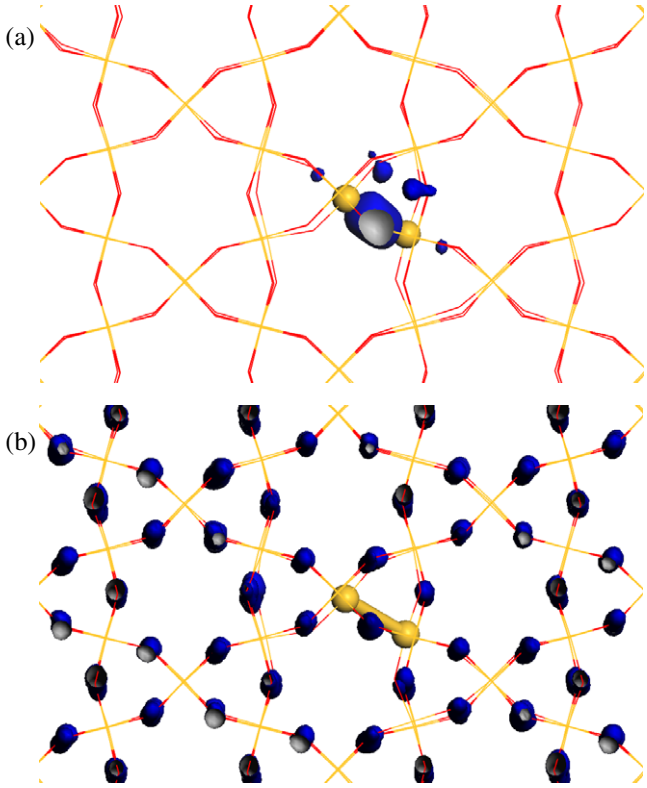

Figure 6. 3D isosurface plot of (a) HOMO at $\rho = 0.02$ and (b) LUMO at $\rho = 0.0005$ for V_O from the $3 \times 3 \times 3$ supercell at 0 GPa.

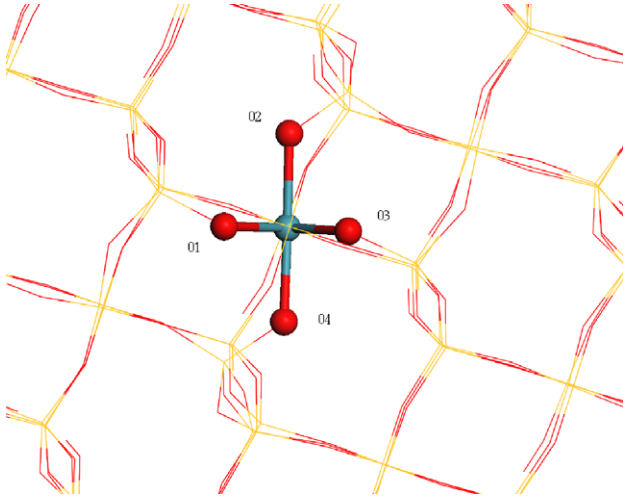

Figure 7. Local structure of the relaxed $Xe@V_{Si}$ defect from the $3 \times 3 \times 3$ supercell at 0 GPa.

Table 9. Local electronic structure of $Xe@V_{Si}$.

P	q^M (Xe)	q^M (O1)	q^M (O2)	q^M (O3)	q^M (O4)	LUMO (eV)
0 GPa	+1.80	−0.96	−1.0	−0.96	−1.0	0.672
2 GPa	+1.82	−0.97	−1.0	−0.97	−1.0	0.810

earlier. The local structure of the $Xe@V_{Si}$ defect at $P = 0$ GPa is shown in figure 7.

Note that, while the initial unrelaxed structure was tetrahedral, the relaxed structure has two long and two short Xe–O bonds. The detailed geometry for the relaxed structure at both $P = 0$ and 2 GPa is given in table 8. This is an unusual conformation, and is clearly more planar than tetrahedral and must be stabilized by the surrounding environment. Indeed, when an isolated XeO_4 molecule is relaxed starting from this initial structure using the same DFT parameters, O1 and O3 are close enough to trigger the dissociation into $O_2 + XeO_2$ with Xe–O bond length 1.882 Å and O–Xe–O angle 123.2°. However, further investigation showed that a pure planar XeO_4 structure is also possible as a gas phase molecule with an Xe–O bond of 1.898 Å and O–Xe–O angles of 90°. This structure is 1.43 eV higher in energy than the pure tetrahedral structure and is metastable as a gas phase molecular conformer.

The local electronic structure of the $Xe@V_{Si}$ defect is detailed in table 9 along with the position of the LUMO, at both $P = 0$ and 2 GPa. The localized nature of the defect states is again visible in the 3D isosurface plot of the HOMO and LUMO at $P = 0$ GPa as shown in figure 8. Comparison of the DOS for $Xe@V_{Si}$ and V_{Si} in figure 4 shows the creation of an additional (localized) defect state in the bandgap at approximately $E_F + 0.7$ eV, and changed weights for the other localized defect states coming from V_{Si}. Whilst it is tempting from the DOS to associate the new state at $E_F + 0.7$ eV with a small shift in the localized state that was previously visible as a small shoulder in the DOS at E_F for the V_{Si} system, this is probably not valid as there has been significant local structural relaxation due to the Xe atom.

3.2.4. Xenon at oxygen vacancy. It is expected that there will be a higher density of V_O sites than V_{Si} sites and hence even though the two-stage energetics would favour the formation of $Xe@V_{Si}$ there should still be an appreciable amount of $Xe@V_O$ present. The local relaxed structure of this defect at $P = 0$ GPa is shown in figure 9. The detailed structure at both $P = 0$ and 2 GPa is given in table 10.

As before, a Mulliken population analysis was performed at both pressures and the electronic DOS calculated; the results are summarized in table 11. A 3D isosurface plot of the HOMO and LUMO at $P = 0$ GPa (as shown in figure 10) again shows the localized nature of the defect states. However, the DOS plots in figure 4 show that this time there has been a significant shift in the Fermi level as the bulk states are now shifted to

Table 10. Local structure of Xe@V_O.

P (GPa)	Si1–Xe (Å)	Si2–Xe (Å)	O1–Xe (Å)	O2–Xe (Å)	O3–Xe (Å)	Si–Xe–Si2 (deg)	Xe–O1–Si2 (deg)	Xe–O2–Si2 (deg)	Xe–O3–Si3 (deg)
0	2.484	3.338	2.999	3.015	2.714	122.6	85.9	85.6	94.6
2	2.482	3.333	2.945	2.986	2.735	124.3	86.1	88.1	94.0

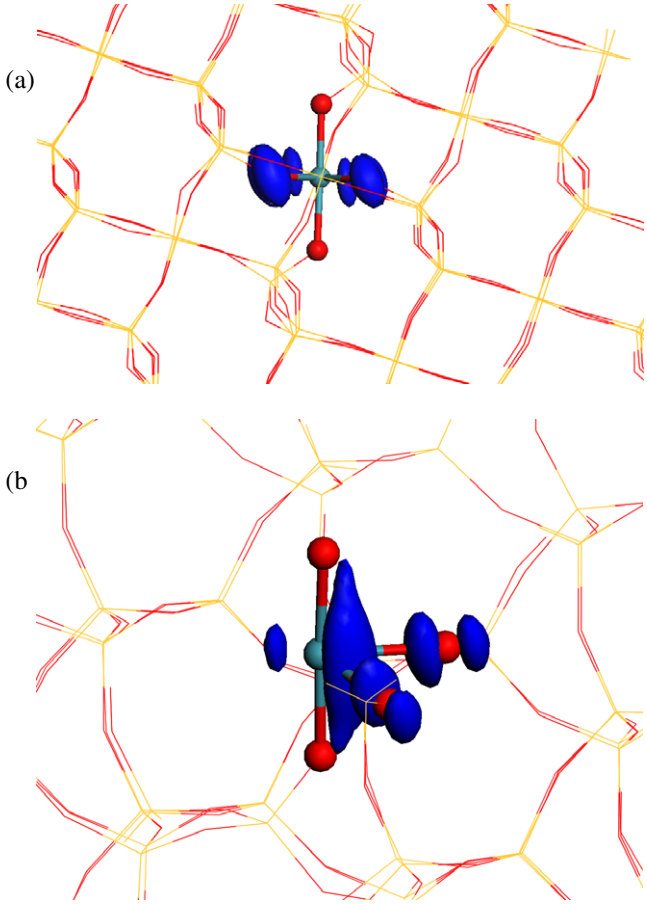

Figure 8. 3D isosurface plot at $\rho = 0.02$ of (a) HOMO and (b) LUMO for Xe@V_{Si} from the $3 \times 3 \times 3$ supercell at 0 GPa.

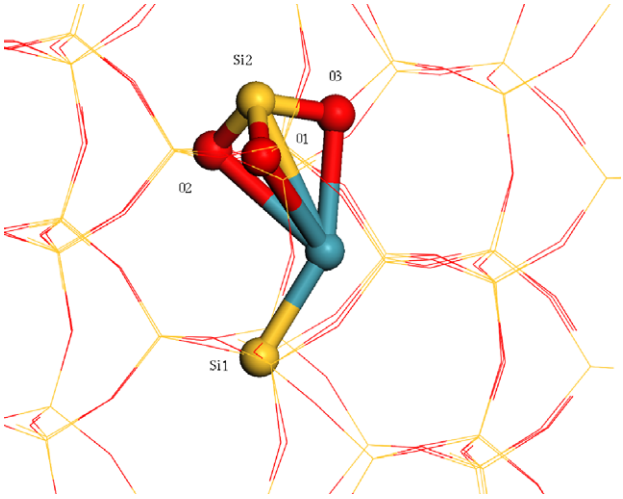

Figure 9. Local structure of the relaxed Xe@V_O defect from the $3 \times 3 \times 3$ supercell at 0 GPa.

below $E_F - 3.0$ eV and the Fermi level is now positioned in a localized defect state. This significantly changes the electronic properties of this defect state. Finally, the LUMO is at $E_F + 2.2$ eV and is clearly distinct from the bulk conduction bands which start at $E_F + 3.0$ eV.

3.2.5. Xenon at the interstitial site. If the Xe absorption is a single-step process, then the interstitial site, Xe@I, has the lowest formation cost. The structure of this defect is shown in figure 11 and detailed in table 12. As for the other defects, a Mulliken population analysis was also performed, along with an electronic DOS—these results are summarized in table 13. A 3D isosurface plot of the HOMO and LUMO at $P = 0$ GPa is shown in figure 12. Note that, whilst the HOMO is still localized, the LUMO is now delocalized as in the case of the V_O defect (hence the need to reduce the isosurface value in this figure). This can be understood from the DOS plots in figure 4 which show little weight of extra states in the bandgap and hence the LUMO corresponds to a delocalized bulk-like state. A detailed comparison of the DOS and integrated DOS for Xe@I and pure α-quartz shows that the additional states from the Xe atom have principally gone into the valence band from $E_F - 4.0$ eV to E_F. Indeed, there is a hint of this in the appearance of a small shoulder in the DOS at E_F seen in both Xe@I and Xe@V_{Si}. The absence of this shoulder in Xe@V_O is probably therefore the mechanism for the first defect state in Xe@V_O appearing at a higher energy and therefore shifting E_F in that system onto the localized states.

4. Conclusion

It has recently been suggested [2] that a significant amount of Xe can be absorbed in α-quartz and that this might be a significant process in the recycling of Xe from the atmosphere to the interior of the Earth. *Ab initio* calculations of Xe absorption in α-quartz have been presented, and analysed in terms of the local atomic and electronic structure. Three distinct candidate sites for the Xe atom were found to be mechanically stable upon lattice relaxation: substitutional at the silicon vacancy (Xe@V_{Si}) or the oxygen vacancy (Xe@V_O) and at an interstitial site (Xe@I). The energetics and electronic properties of these defect structures are analysed and it is shown that there is an energy barrier to the absorption at all sites at $T = 0$. If the Xe absorption is a single-stage process in a perfect crystal then the lowest formation energy barrier (at both $P = 0$ and 2 GPa) is at the interstitial site. If it is a two-stage process (as possible for both the vacancy sites if the vacancies were already present as intrinsic point defects)

Table 11. Local electronic structure of Xe@V_O.

P (GPa)	q^M (Xe)	q^M (Si1)	q^M (Si2)	q^M (O1)	q^M (O2)	q^M (O3)	LUMO (eV)
0	+0.55	+2.12	+1.12	−1.16	−1.17	−1.16	2.220
2	+0.56	+2.11	+1.14	−1.16	−1.18	−1.16	2.336

Table 12. Local structure of Xe@I.

P (GPa)	O1–Si1 (Å)	O2–Si1 (Å)	Si1–Xe (Å)	Si2–Xe (Å)	O3–Si2 (Å)	O4–Si2 (Å)	O1–Si1–O2 (deg)	O3–Si2–O4 (deg)	Si1–Xe–Si2 (deg)
0	1.625	1.626	2.937	2.945	1.623	1.626	121.5	121.7	148.9
2	1.614	1.616	2.983	2.985	1.613	1.615	120.3	120.4	147.4

Table 13. Local electronic structure of Xe@I.

P (GPa)	q^M (Xe)	q^M (Si1)	q^M (Si2)	q^M (O1)	q^M (O2)	q^M (O3)	q^M (O4)	LUMO (eV)
0	+0.39	+2.27	+2.28	−1.16	−1.17	−1.16	−1.17	5.412
2	+0.39	+2.28	+2.28	−1.17	−1.17	−1.17	−1.17	5.575

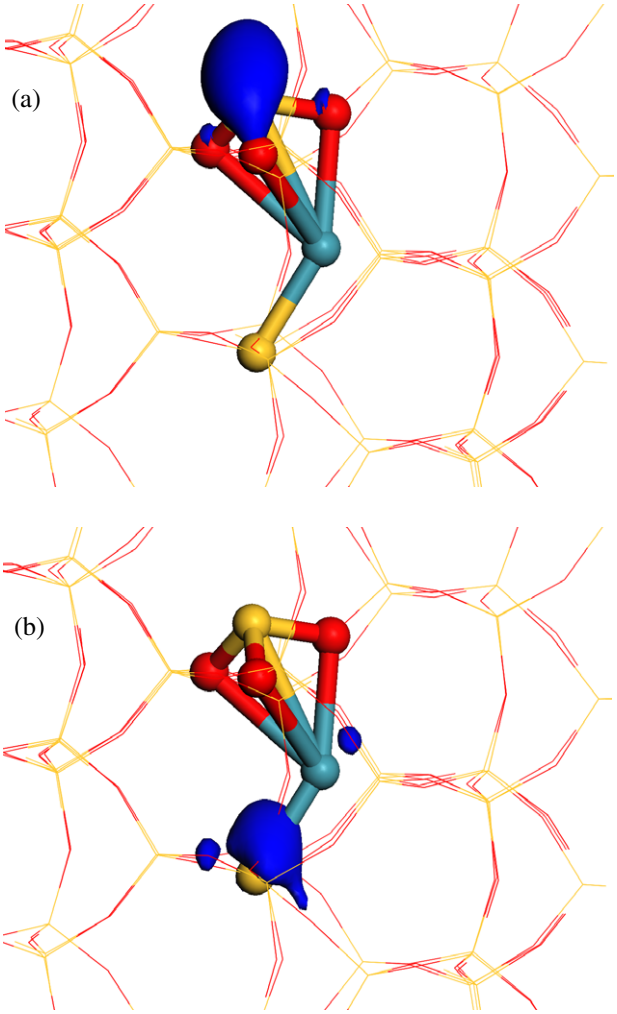

Figure 10. 3D isosurface plot at $\rho = 0.02$ of (a) HOMO and (b) LUMO for Xe@V_O from the 3 × 3 × 3 supercell at 0 GPa.

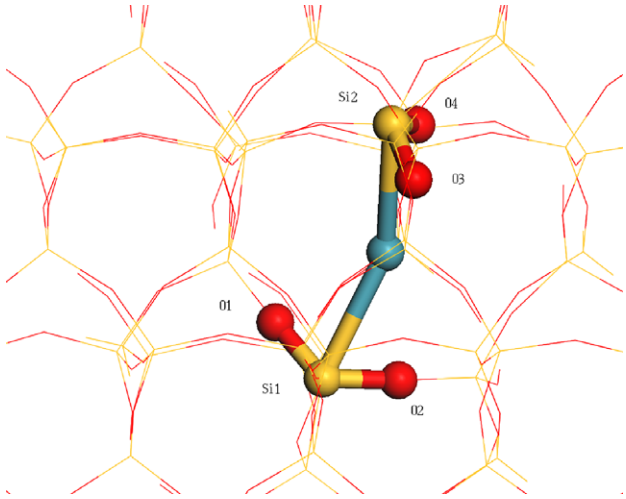

Figure 11. Local structure of the relaxed Xe@I defect from the 3 × 3 × 3 supercell at 0 GPa.

then the subsequent barrier is much lower and Xe@V_{Si} has the lowest formation energy. However, the silicon vacancy has a considerably higher formation energy than the oxygen vacancy in a quartz-rich environment, as found inside the Earth, and hence it should be expected that there will be a much higher density of oxygen vacancies available for Xe absorption. A comparison to the work of Richard *et al* [23] on vacancies in amorphous SiO_2 structures shows that the results here should be transferable to a wide range of similar SiO_2 structures. Hence in a realistic, defective sample of α-quartz or other similar SiO_2 polymorphs at high temperature and pressure it is to be expected that all three candidate sites should be occupied. In this paper, the structure and electronic properties of these three distinct defect sites in α-quartz have been studied. As the electronic properties of these sites have been shown to be quite distinct, it is possible that these different possibilities could be tested using EPR or some other local electronic spectroscopy.

This work therefore confirms the basic tenet of [2]: α-quartz *can* absorb a high wt% of Xe under Earth core conditions (high temperature and pressure), but there are three possible candidate sites, not just the one previously suggested. This offers an interesting possible answer to the question of

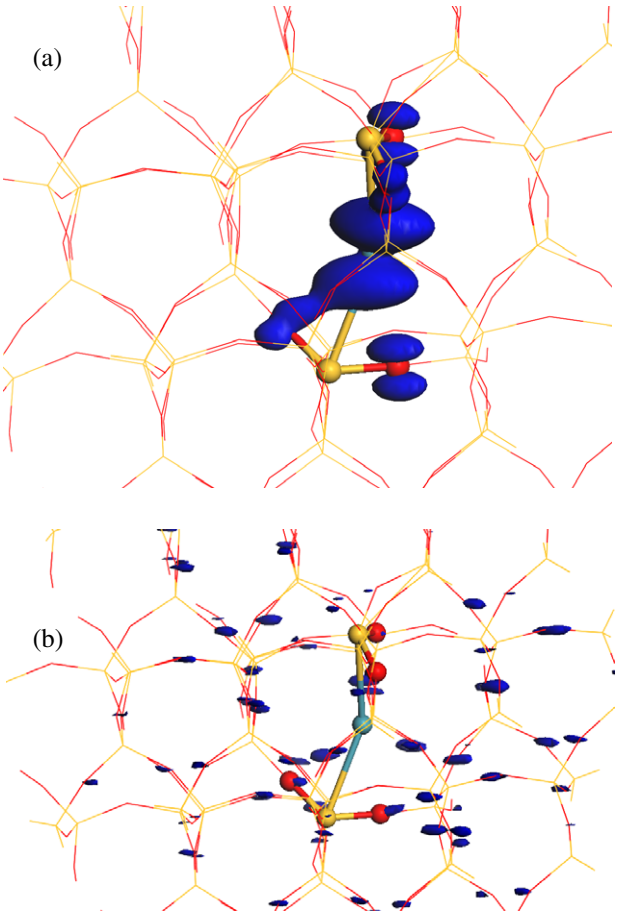

Figure 12. 3D isosurface plot of (a) HOMO at $\rho = 0.02$ and (b) LUMO at $\rho = 0.0008$ for Xe@I from the $3 \times 3 \times 3$ supercell at 0 GPa.

'where has all the missing Xe gone?' This work also shows that none of these defects are stable at $T = 0$, which therefore explains the degassing of Xe from magma at the surface of the Earth as seen in [8].

Acknowledgments

This work was performed using the Darwin Supercomputer of the University of Cambridge High Performance Computing Service (http://www.hpc.cam.ac.uk/), provided by Dell Inc. using Strategic Research Infrastructure Funding from the Higher Education Funding Council for England. The author would like to acknowledge the University of York 40th Anniversary Lectureship scheme for sabbatical leave which enabled this study.

References

[1] Anders E and Owen T 1977 Mars and Earth—origin and abundance of volatiles *Science* **198** 453–65
[2] Sanloup C, Schmidt B C, Perez E M C, Jambon A, Gregoryanz E and Mezouar M 2005 Retention of xenon in quartz and Earth's missing xenon *Science* **310** 1174–7
[3] Kunz J, Staudacher T and Allegre C J 1998 Plutonium-fission xenon found in Earth's mantle *Science* **280** 877–80
[4] Caldwell W A, Nguyen J H, Pfrommer B G, Mauri F, Louie S G and Jeanloz R 1997 Structure, bonding, and geochemistry of xenon at high pressures *Science* **277** 930–3
[5] Wacker J F and Anders E 1984 Trapping of xenon in ice—implications for the origin of the Earth's noble-gases *Geochim. Cosmochim. Acta* **48** 2373–80
[6] Sill G T and Wilkening L L 1978 Ice clathrate as a possible source of atmospheres of terrestrial planets *Icarus* **33** 13–22
[7] Matsuda J and Matsubara K 1989 Noble-gases in silica and their implication for the terrestrial missing Xe *Geophys. Res. Lett.* **16** 81–4
[8] Holland G and Ballentine C J 2006 Seawater subduction controls the heavy noble gas composition of the mantle *Nature* **441** 186–91
[9] Pettersson M, Lundell J and Räsänen M 1999 New rare-gas-containing neutral molecules *Eur. J. Inorg. Chem.* **1999** 729–37
[10] Sanloup C, Mao H K and Hemley R J 2002 High-pressure transformations in xenon hydrates *Proc. Natl Acad. Sci. USA* **99** 25–8
[11] Segall M D, Lindan P J D, Probert M J, Pickard C J, Hasnip P J, Clark S J and Payne M C 2002 First-principles simulation: ideas, illustrations and the CASTEP code *J. Phys.: Condens. Matter* **14** 2717–44
[12] Clark S J, Segall M D, Pickard C J, Hasnip P J, Probert M J, Refson K and Payne M C 2005 First principles methods using CASTEP *Z. Kristallogr.* **220** 567–70
[13] Payne M C, Teter M P, Allan D C, Arias T A and Joannopoulos J D 1992 Iterative minimization techniques for *ab initio* total-energy calculations—molecular-dynamics and conjugate gradients *Rev. Mod. Phys.* **64** 1045–97
[14] Probert M I J 2003 Molecular dynamics studies of liquids using a Beowulf computer *Contemp. Phys.* **44** 435–50
[15] Perdew J P 1991 *Electronic Structure of Solids '91* ed P Zeische and H Eschrig (Berlin: Akademie)
[16] Vanderbilt D 1990 Soft self-consistent pseudopotentials in a generalized eigenvalue formalism *Phys. Rev.* B **41** 7892–5
[17] Pfrommer B G, Cote M, Louie S G and Cohen M L 1997 Relaxation of crystals with the quasi-Newton method *J. Comput. Phys.* **131** 233–40
[18] Gunderse G and Hedberg K 1970 Molecular structure of xenon tetroxide, XeO_4 *J. Chem. Phys.* **52** 812
[19] Segall M D, Shah R, Pickard C J and Payne M C 1996 Population analysis of plane-wave electronic structure calculations of bulk materials *Phys. Rev.* B **54** 16317–20
[20] Carbonaro C M, Fiorentini V and Massidda S 1997 *Ab initio* study of oxygen vacancies in alpha-quartz *J. Non-Cryst. Solids* **221** 89–96
[21] Pacchioni G 2000 *Ab initio* theory of point defects in oxide materials: structure, properties, chemical reactivity *Solid State Sci.* **2** 161–79
[22] Sulimov V B, Sushko P V, Edwards A H, Shluger A L and Stoneham A M 2002 Asymmetry and long-range character of lattice deformation by neutral oxygen vacancy in alpha-quartz *Phys. Rev.* B **66** 024108
[23] Richard N, Martin-Samos L, Roma G, Limoge Y and Crocombette J P 2005 First principle study of neutral and charged self-defects in amorphous SiO_2 *J. Non-Cryst. Solids* **351** 1825–9
[24] Choudhury N and Chaplot S L 2006 *Ab initio* studies of phonon softening and high-pressure phase transitions of alpha-quartz SiO_2 *Phys. Rev.* B **73** 094304